Hindawi Publishing Corporation
Advances in Tribology
Volume 2008, Article ID 325187, 16 pages
doi:10.1155/2008/325187

Research Article

Film Thickness Analysis for EHL Contacts under Steady-State and Transient Conditions by Automatic Digital Image Processing

E. Ciulli,[1] T. Draexl,[2] and K. Stadler[1]

[1] *Dipartimento di Ingegneria Meccanica, Nucleare e della Produzione, Università degli Studi di Pisa, Via Diotisalvi 2, 56126 Pisa, Italy*
[2] *Forschungsstelle für Zahnräder und Getriebebau, Lehrstuhl für Maschinenelemente, Technische Universitaet Muenchen, Boltzmannstraße 15, 85748 Garching, Germany*

Correspondence should be addressed to E. Ciulli, ciulli@ing.unipi.it

Received 18 April 2007; Accepted 7 August 2007

Recommended by M. Kaneta

The knowledge of the film thickness values is very important in lubricated contacts to verify the lubrication conditions. Optical interferometry is one of the most used methodologies for film thickness and shape determination of Elastohydrodynamic-lubricated contacts. An image processing programme has been developed for the analysis of white light interferograms. The programme, based on the analysis of the hue channel, has been developed in order to process big amounts of images, as often generated under transient conditions. The measurement range is currently limited to a maximum film thickness of 0.7 μm. The programme has been used for analysing several images recorded in tests carried out with a ball on disc contact under steady-state as well as transient conditions for different velocities and slide-to-roll ratios. Under transient conditions, the entraining velocity is varied with a sinusoidal law for two different frequencies. The results obtained evidenced an asymmetric reduction of the film thickness when increasing the percentage of sliding, both for stationary and transient conditions. Under transient conditions with increasing test frequency, film thickness loops of increasing amplitude have been found that reduce their amplitude more when the ball is running faster than the disc. Squeeze and thermal effects can explain the results obtained.

1. INTRODUCTION

Film thickness measurements of Elastohydrodynamic (EHD) lubricated contacts are important to evaluate the lubrication regime. One of the most used methods of film thickness investigation is optical interferometry. This method has been successfully applied to EHL contacts since the 1960s and is particularly suitable for determining also the shape of an EHL contact. The first investigations were made under pure sliding and pure rolling conditions using experimental rigs with contacts between balls and plates [1, 2].

Some of the typical EHD-lubricated machine elements, as rolling element bearings, cams or gears, work under conditions where thermal effects due to sliding are not negligible. Furthermore, it must be considered that machine elements are working mainly under transient conditions by means of changing radius of curvature, load, or speed. Therefore, experimental investigations have been successively made including sliding effects by testing different values of the slide-to-roll ratio S or by testing under transient conditions. Just to mention some of these studies, Smeeth and Spikes [3] investigated the behaviour of S on an EHL point contact for different oils by analysing the film thickness, and Sugimura et al. [4] investigated the effect of squeeze on the film thickness under transient conditions (but the effect of S was not included).

More recently, the authors investigated nonconformal lubricated contacts between steel balls and glass discs for different S also under transient conditions [5, 6]. These previous works were more addressed to friction investigation and showed the need of further investigations and a better film thickness analysis. Particularly under transient conditions, a huge amount of interference images were recorded that could

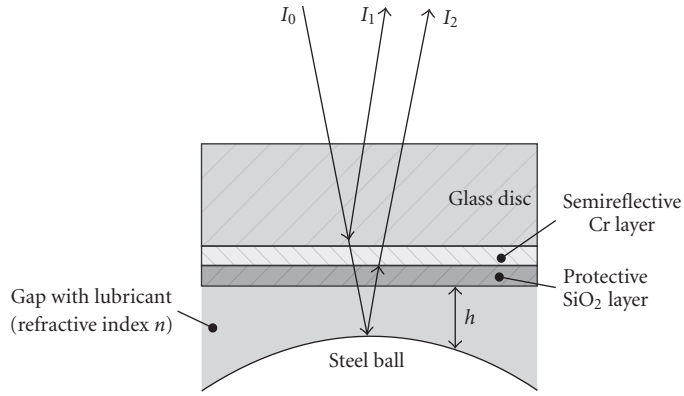

Figure 1: Basic principle of interferometric film thickness measurement.

not be analysed efficiently by eye and an automatic method was considered to be necessary.

Some programmes for almost automatic analysis of monochromatic interference images have been already developed, as reported in [7, 8]. However, for reasons of a better resolution and higher light intensity, related to the reduced exposure time necessary for recording images under transient conditions, the use of interference filters for monochromatic interferometry is not preferable; white light interference, producing colour images, was therefore used for this kind of tests.

In this work, the main aspects of the programme developed capable of determining the local lubricant film thickness in the entire area of an EHL point contact are described. The programme can process large series of images with a moderate amount of user inputs. For the automatic analysis of white light interferograms different methods exist. One recent method is based on the analysis of the RGB colour space [9], whereas the other method uses the HSV colour space [10]. The latter image processing method first introduced by Marklund is used due to its greater simplicity and minor sensitivity to illumination conditions. The programme developed is tested by analysing interference images obtained in tests carried out under conditions similar to previous works [5, 6]. The film thickness results obtained both under stationary and transient conditions for different S are presented and analysed.

2. PROCESSING OF WHITE LIGHT INTERFEROGRAMS

2.1. Basic aspects of optical interferometry applied to EHL contacts

As well known, for the investigation of EHL contacts, monochromatic and white light interferometry is often used. In both cases images with fringes are formed by the interference of the beams reflected by the two surfaces of the contacting bodies separated by the lubricant. Images with dark and bright fringes are formed by the light of one determined wavelength (monochromatic interferometry) whereas a spectrum of coloured fringes is formed by white light interferometry.

The basic principle of the formation of interference patterns for monochromatic interferometry is shown in Figure 1.

In common EHL investigations, a glass disc is used coated with a semireflective chromium layer on the side of the contact. A beam of light falling through the glass will be partially reflected at the interface between the glass and the chromium layer, whereas another part will go through it and is reflected at the surface of the specimen. The silica (SiO_2) layer shown in Figure 1 serves as protection to reduce abrasion and also as a spacer layer to extent the lower measurement range. Since the two beams cover different distances, there will be a phase shift between the corresponding light waves. When the waves superimpose, the resulting amplitude will be between zero (destructive interference) and twice the amplitude of the original wave (constructive interference), depending on the optical retardation. Thus, an interference pattern consisting of bright and dark fringes can be made visible in the monochromatic case and multicolour fringes using white light interferometry.

Film thickness values are then evaluated when using monochromatic interferometry knowing the wavelength of the light and the refractive index of the lubricant considering the fringes order. The resolution is limited since normally only discrete film thicknesses at the bright and dark extremes can be calculated and the values in between must be interpolated. The distance of these discrete values for the commonly used light's wavelength and lubricant's refractive index is in the order of 90 nm.

In white light interferometry, every coloured fringe corresponds to a certain film thickness and this usually provides a better resolution than monochromatic interferometry. Considering that the correlation between film thickness and any numerical representation of colours is generally nonlinear, film thicknesses can be determined by a table lookup once an appropriate calibration table is available. The greatest disadvantage of white light interferometry is a rather strict limitation of the measurement range. Film thicknesses smaller than about 0.1 μm tend to appear as shades of grey (with zero theoretically resulting in black), and above roughly 1 μm fringes are not visible at all due to the low-coherent nature of white light. The lower limit can

be extended by adding a spacer layer of transparent material to the disc (often referred to as ultra thin interferometry), but this implicates an equivalent reduction of the upper limit. Although the measurement range is rather narrow, it is in the scale of common EHL film thicknesses.

First methods using white light interferometry are based on the human ability to compare the colours with a calibration table. It should be noted that colour perception may vary from person to person and thus "manual" analysis of white light interferograms should be taken with care and needs a lot of time and experience.

Successively, some methods have been developed to correlate the colour information stored in the recorded images to the film thickness in more or less automatic ways.

There are several ways of describing colour information quantitatively for processing on computers. RGB colour space is the most common one, since it represents each colour by its red, green, and blue component. Another colour space, which is to some extent closer to the human perception of colour, is known as HSV. Identical or very similar colour spaces are sometimes also referred to as HSB, HSI, HSL, or θ-S-W. It defines colour by its hue H, saturation S, and value V components. RGB and HSV can be converted into each other by a nonlinear, bijective transformation. Out of the HSV space, only the H channel is used due to its insensitivity to luminance and saturation of the colours, which are stored in the two other channels. Therefore, the measurement results are unlikely to be influenced by illumination conditions. In contrast to H, S, and V will change in a very irregular manner within a comparatively small bandwidth and therefore their analysis does not seem eligible for the measurements [11].

Full details of methods on how to use HSV and the H channel in particular for film thickness measurements can be found in [10–13]. Here only the main aspects are reported for understanding the methodologies used in the programme specifically realised for fast processing of image series from experiments under transient conditions.

The value of the H channel can be obtained from R, G, and B [10] by the equation

$$H = \arctan2\left(\frac{2G - R - B}{R - B}\right), \tag{1}$$

where arctan2 is the four-quadrant inverse tangent, which requires a case differentiation depending on the quadrant of the argument.

In a white light interferogram, the progression of the H value over film thickness will be a wrapped signal similar to a periodical signal, but not exactly periodical. Since it can be regarded as a phase angle modulo 2π, it will jump from its minimum to its maximum value or vice versa. A function bounded to the interval $(0, 2\pi)$ can be considered as a wrapped phase signal if it has a progression as shown in Figure 2. In this example, the hue values have been actually calculated using three wavelengths ($\lambda_1 = 505\,\text{nm}$, $\lambda_2 = 540\,\text{nm}$, and $\lambda_3 = 580\,\text{nm}$); H values have been normalised to $(0, 1)$.

If a way is found to deal with the ambiguity of the H values, a calibration table correlating them directly to film thicknesses can be created. This is done by an algorithm that adds (or subtracts, respectively) the height of the interval to all values subsequent to a discontinuity, so that a continuous signal is reconstructed. This process, which is referred to as phase unwrapping, can also be accomplished by computing the numerical derivative (or gradient for phase maps), setting it to zero at the peaks resulting from the discontinuities and reintegrating it. Figure 2 also shows a characteristic behaviour of the unwrapped hue value as a function of the film thickness. The hue value monotonically decreases until a minimum, the position of which depends on the spectrum of the light. For trichromatic light, as assumed in this example, the minimum will usually be above one micron, whereas for white light it is expected between 0.6 and 0.8 microns with a similar course of the function as shown here. As soon as the hue values are available as a monotonic functions in this interval, a calibration table associating them uniquely to film thicknesses can be built straightforwardly. The monotonically increasing section beyond the minimum can only be used for calibration if an additional case differentiation is made.

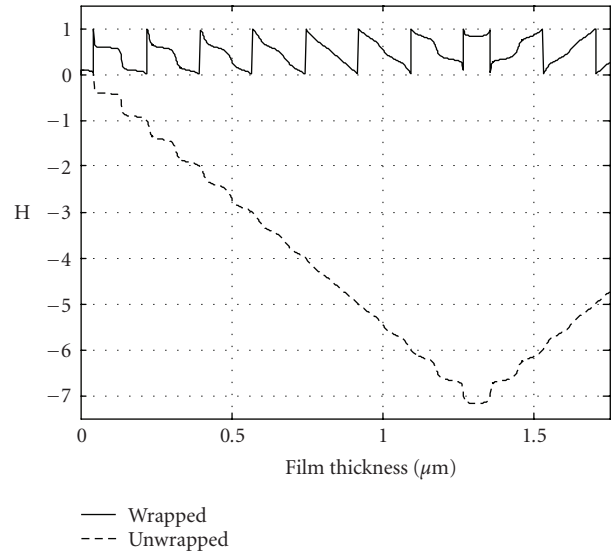

Figure 2: Example of phase wrapped and unwrapped hue values as a function of film thickness.

The hue values in interferograms with repetitive coloured fringes are obviously such functions in two dimensions that will be called wrapped and unwrapped phase maps. An example of a wrapped phase map extracted from a white light interferogram of a real EHL contact is shown in Figure 3(a).

The wrapped hue values in Figure 3 are created by measurements and not by artificially wrapping an unbounded signal as seen in Figure 2. Measurements imply a certain amount of noise and uncertainty. In addition, if the sampling rate is too low, it is possible that the dynamics of the jumps are not fully captured. Therefore, the real jump discontinuities will not be exactly 1 but slightly smaller. Taking into account that the fringes tend to attenuate at large film thicknesses, these effects can become very distinct. Figure 3(b) shows a horizontal section through the wrapped phase map (H value) of Figure 3(a). It is clearly visible that the

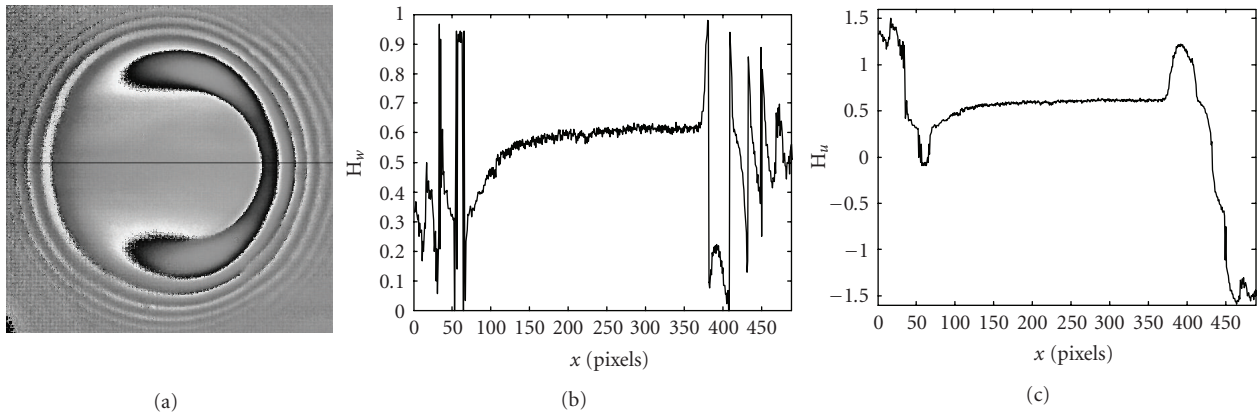

Figure 3: Wrapped phase map of a white light interferogram of an EHL point contact (a) and wrapped (b) and unwrapped (c) hue values along the horizontal line.

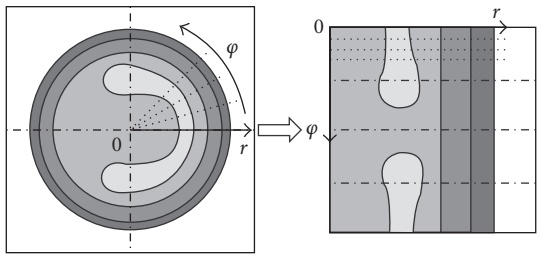

Figure 4: Schematic illustration of the coordinate transformation performed before phase unwrapping.

signal-to-noiseratio and the dynamic range deteriorate towards the edges of the interferogram. Unwrapping such a signal can be challenging, since a discrete signal by definition has discontinuities everywhere. Consequently, it must be decided which of them are caused by actual phase jumps and which by the natural course of the signal, including noise. Low-pass filtering does not solve this problem, since it both reduces noise and smears out the phase jumps, which are high-frequency components themselves. The (partially) unwrapped phase in this particular example is shown in Figure 3(c). The decision criterion (threshold) used in this work has been a discontinuity of more than 0.3 between two consecutive values. In the result, the approximate shape of the typical mid-plane profile of an EHD contact becomes visible (however, in this particular example, the algorithm failed to perform correct unwrapping of the values near the left edge of the plot).

For measured phase maps in two dimensions another important problem arises. Line integrals over them will in general be pathdependent and errors will propagate, making it difficult to obtain an unwrapped result that is consistent everywhere. Since multidimensional phase unwrapping is a task that occurs in various applications, such as magnetic resonance imaging or radar interferometry, various rather complex algorithms have been developed for it in the past. For example, the algorithm presented in [14] had received particular attention and was an important basis for the further developments conducted in [10, 12]. Several versions of the algorithms found in the literature have been implemented in the Matlab environment and tested with interference images obtained with the experimental apparatus described in the following (e.g., [15]). However, none of the algorithms performed satisfactorily on the real interferograms of EHL contacts used. Therefore, a pseudo-two-dimensional integration approach has been finally chosen taking into account that a path-following integration method is likely to produce less inconsistencies if it uses several separate paths that all start at the same point. The two-dimensional unwrapped phase map is assembled by joining the results of all the one-dimensional integrations and interpolating the values that were not covered by any path. Since a method especially for circular point contacts was to be developed, the central point of the contact area suggested itself as the origin for integration paths running radially outwards. In order to obtain a more concise, easy to handle programme code, the algorithm does not operate directly on the original wrapped phase map. In a preprocessing step, the matrix is read out along a sequence of radial lines at intervals of a predefined angular increment. The values retrieved along each of the lines are written into rows of a new matrix. Thus the first column of this matrix will contain the wrapped value of the central point in every row, while the last column will contain the values occurring around the whole circumference of a circle with the maximum radius considered. This transformation is illustrated in Figure 4. Unwrapping itself is accomplished by a simple one-dimensional algorithm that unwraps the preprocessed matrix row by row and decides where to add or subtract integer values (because all wrapped $H \in (0, 1)$) by comparing the differences between consecutive elements to a threshold value T< 1. The threshold value is given to the function as a parameter. Finally, the resulting unwrapped matrix is transformed back into the original coordinates.

Filtering and interpolation operations can be included at this point to reduce the inherent noise of the measured interferograms. For all filtering operations, spatial averaging by convolution with a finite impulse response (FIR) filter was

implemented. This filter replaces every matrix element by a (weighted) average of its neighbours [16]. Mathematically, this can be described by the convolution sum

$$\widetilde{\mathbf{A}}_{m,n} = \sum_k \sum_l \mathbf{F}_{k,l}\, \mathbf{A}_{m-k,\,n-l}, \tag{2}$$

where $\mathbf{A} = \{A_{m,n}\}$ and $\widetilde{\mathbf{A}} = \{\widetilde{A}_{m,n}\}$ are the matrices containing the input and output values respectively, and $\mathbf{F} = \{f_{k,l}\}$ is the convolution kernel or filter mask that defines the filter. Uniform convolution kernels, consisting of an $N \times N$ matrix with each element $f(k,l) = 1/N^2\, \forall (k,l)$, turned out to deliver good results, that is, they effectively reduce noise without changing the low-frequency components of the signal.

This pseudo-two-dimensional algorithm is stable as long as the threshold value is not set smaller than twice the maximum noise amplitude that occurs in the matrix. The simple arithmetic without any calculations in the frequency domain does not cause undesirable oscillations in the result. The success of the unwrapping procedure will depend on the quality of the input image, in particular on the magnitude of the phase discontinuities and the signal-to-noise ratio.

2.2. Organisation of the image processing software

For the software realised, Matlab has been chosen as the programming environment because it offers built-in functions for image and signal processing, as well as versatile data input and output capabilities.

The software follows a calibration-lookup approach. The necessary operations to obtain film thicknesses from interferograms can be split up into two main steps. First, a correlation between film thicknesses and hue values, that is, a calibration table, must be found. In a second step, the actual image analysis, this calibration table can in turn be applied to determine film thicknesses from given hue values. In both cases, phase unwrapped hue values are used. Since the calibration procedure must be accomplished at most once per experiment, the two subtasks were realised in separate programs (Figure 5). Both of them employ the same unwrapping algorithm, but differ slightly in the way they process images. This is due to the fact that for calibration the area outside of the actual (Hertzian) contact is of interest, whereas for image analysis mainly the (EHL) contact zone itself is considered.

The calibration programme *calibration.m* requires as input an interferogram image of a Hertzian point contact and a table containing the height of the gap around this contact as a function of the radius around its centre. The output is a Matlab file containing the calibration lookuptable. The parameters requested as user inputs include the area within the image to use and the scaling factor relating the size of a pixel in the image to the corresponding length in the real contact. In consideration of the programme being comparatively seldom used, further interaction with the operator is intended to ensure that only correctly phase unwrapped values are exploited.

In contrast, the image processing programme *wliproc.m* (white light interferogram processor) passes on fewer decisions to the operator. A set of parameters for each experiment must be given at the beginning. Once an image file name is provided to the programme, it looks for all files generated by the camera software. So there is no need to open every interferogram separately. This batch-processing feature is meant when processing several images in succession. A limited number of partially graphical inputs must be made until the calibration table can be applied and the result is visualised. If the user accepts it, a result file in Matlab format and several figures are created. The raw, unwrapped hue values are also saved in case the calibration table should turn out to be erroneous later.

2.3. Consideration on accuracy

The calibration table is presented as a diagram like in Figure 6.

The resolution of the calibration table depends on the resolution of the given hue values. For a 24-bit colour image, each channel (R, G, B or H, S, V) is represented by 8 bits and can thus adopt 255 discrete values. By phase unwrapping, which extends the width of the range of values from 1.0 to approximately 3.2, this number is extended to more than 800 values in the present example. They are distributed over a film thickness range of 0.7 μm. If the calibration functions were assumed to be linear, the corresponding film thickness difference between two discriminable colours would be 0.7 μm/800 <1 nm. Theoretically, this value could even be improved by recording and processing images of a higher-colour depth (the present camera is capable of producing 10 bits per channel). However, the influence on the resolution by other factors is significantly higher.

For example, the spatial resolution with which the interference pattern is recorded must be taken into account. The distance between two pixels in the image equals 1.18 μm here. The steepest slope of the steel ball's contour used within the measurement range is about $\Delta h/\Delta r \approx 0.005$. Thus, the largest vertical distance between two points mapped to neighbouring pixels will be $0.005 \times 1.18\,\mu\text{m} \approx 6$ nm. However, for some ranges of values, the resolution might also be limited due to the nonlinear nature of the calibration function. Between 0.16 and 0.24 μm the curve is relatively steep, that is, a small change of the hue value corresponds to a large film thickness difference. This range is covered by roughly 20 discrete hue values, resulting in a resolution of about 4 nm. Furthermore, the shape of the Hertzian contact assumed for the calibration results from a theoretical model, whereas the real shape may deviate from the theory due to manufacturing inaccuracy and surface roughness. The surface roughness of the steel ball (mean-square-roughness R_q) was given to be 8 nm here.

Taking all these considerations into account, one can expect an uncertainty of measurement in the order of 10 nm. This assumption was tested by analysing several interferograms of different Hertzian contacts by the processing programme comparing calculated and theoretical results.

The calibration images are recorded at atmospheric pressure (the area of interest is outside the Hertzian contact), whereas the pressure in the lubricant film of an EHL contact is much higher. Moreover, pressure varies considerably

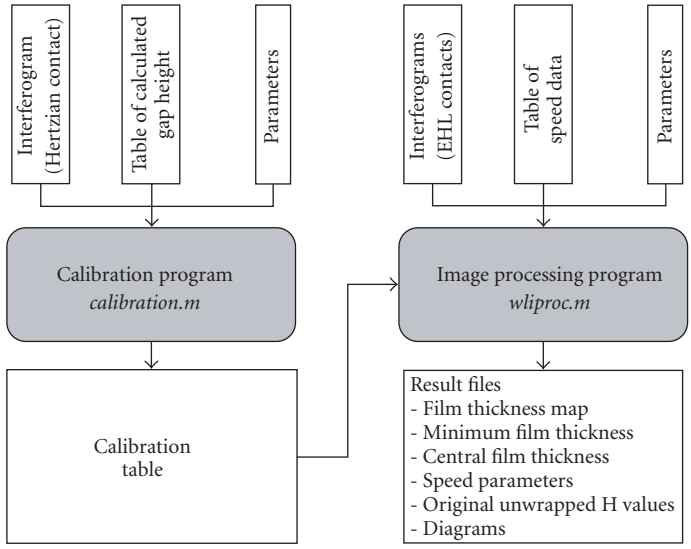

Figure 5: Structure of the two main programs and their interaction.

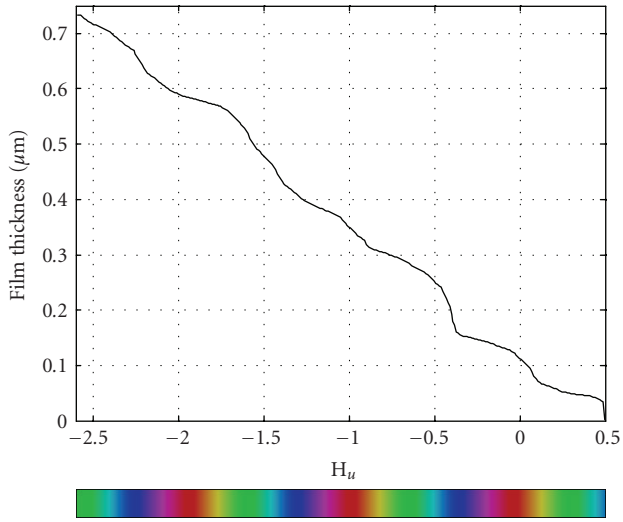

Figure 6: Calibration curve uniquely associating film thicknesses to unwrapped H values. The corresponding colours are shown in the colour bar (only hues, not considering possible variations of saturation and luminance).

within the contact area, causing locally varying deviations of the measured film thickness. These errors can be dealt with if algorithms are employed that calculate the pressure distribution from the initially measured film thicknesses. In an iterative correction scheme film thickness and pressure can then be redetermined until the procedure converges and further changes become insignificant. Such correction methods based on a pressure-density model and the Lorentz-Lorentz relation have been reported in [9, 17]. In the present version of the program, which concentrates on film thickness determination itself, a refractive index correction is not implemented yet.

In [9], a change of the film thickness after several iterations of 6% was reported for the area of the outlet constriction where the maximum pressure occurs. The authors used parameters very similar to those adopted in the present work. Therefore, the errors are assumed to lie in the same scale and thus also in the scale of the method uncertainty of measurement.

The methodology developed needs still to be improved. However, despite its limitations, a necessary important first step for the comparison between steady-state and transient conditions result is done.

2.4. Example of programme use

To illustrate how the film thickness is obtained from an interferogram as provided by the camera, the main steps and intermediate results are described in the following.

A sample white light interferogram has been selected that presents some light intensity differences for showing the capabilities of the programme developed (Figure 7(a)). After the image is provided as an input to the programme together with the actual pixel dimension and the calibration table, a version of the image with enhanced colours is created to facilitate the selection of the central point (Figure 7(b)).

After selecting the centre of the interferogram, phase unwrapping of the H channel is started with an initial threshold value; if results are unsatisfactory, different values can be chosen. Results obtained with an initial threshold value of 0.25 and a successive value of 0.2 are shown in Figure 8. A good portion of the contact zone is reproduced well in Figure 8(a) besides the peaks visible near the edge of the processed area. In this region, the dynamic range of the H signal is compressed too much to be unwrapped successfully. However, most of these points lie outside the measurement range anyway and would be excluded from further processing. A disturbing phenomenon can be observed looking at Figure 8(a),

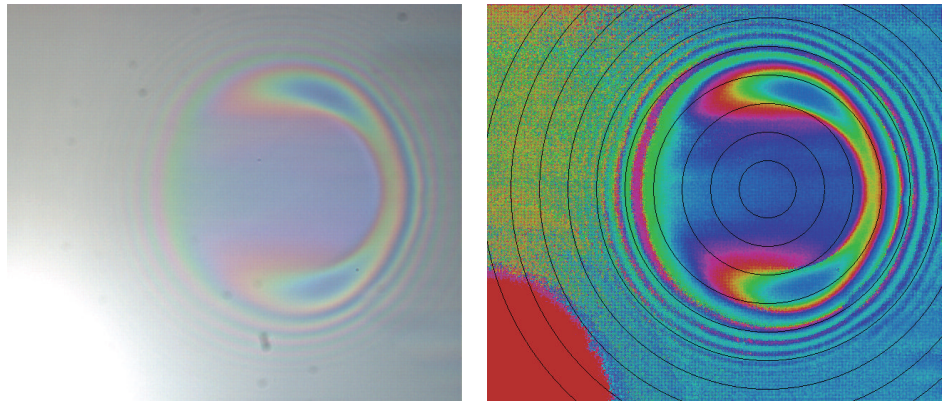

(a) (b)

Figure 7: White light interferogram of an EHL point contact as recorded by the camera (a) and image with enhanced colours and circles displayed to facilitate the selection of the central point (b).

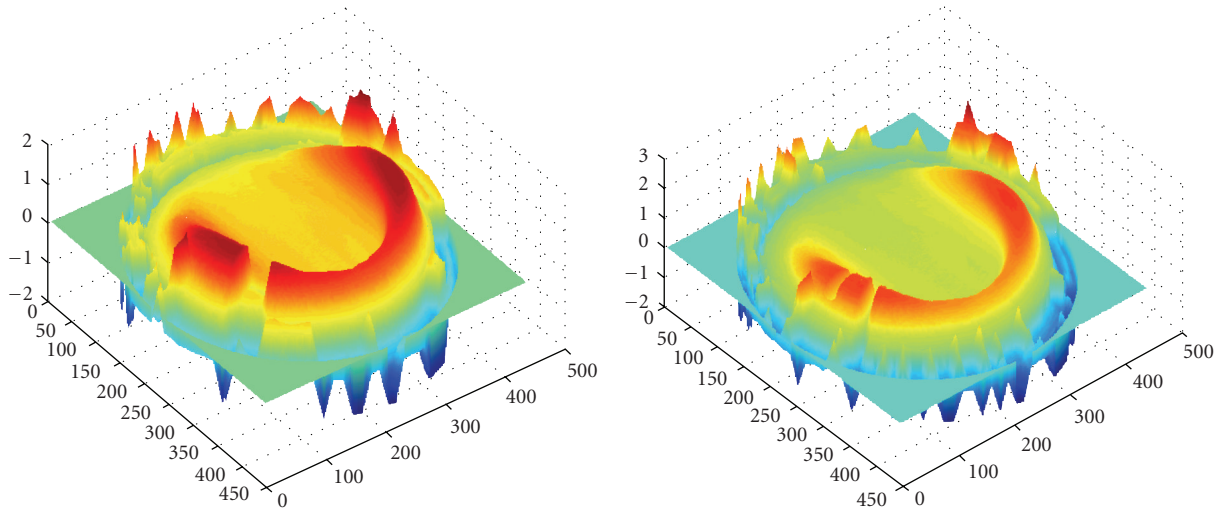

(a) (b)

Figure 8: Phase unwrapped H channel obtained using a threshold value of 0.25 (a) and of 0.2 (b).

a gap appearing in one of the side lobes located close to the zone of minimum film thickness.

Adjusting the unwrapping threshold can improve the result (Figure 8(b)), but the error cannot be completely eliminated in this case. Thoroughly looking at the image, the reason becomes evident. Figure 7(b) shows that between the blue central zone and the green fringe in the zone of minimum film thickness there are purple, red, and yellow fringe. However, these fringes seem to be noncontinuous at the inner edge of the lower-side lobe. Here, an almost direct transition from blue to green occurs. Thus, there is no conspicuous discontinuity between the wrapped H values of neighbouring pixels, causing the unwrapping algorithm to fail. This localised absence of colours is assumed to be related to the present optical equipment.

Before offering the option to use only the flawlessly unwrapped half of the results, the programme asks the user to define up to what radius the data will be used as input for film thickness calculation. This radius is chosen by mouse click in such a way that the largest possible area is covered without including points beyond the measuring range or distortions caused by failed phase unwrapping (Figure 9). Similar to the selection of the central point, the choice is shown as a circle in the image. The last user input before actually determining film thicknesses is a mouse click on the point where minimum film thickness is assumed to be. Since the film thickness in the calibration table is a strictly monotonic function of the unwrapped hue value, this decision can already be taken before any film thicknesses are known.

After adding a spherical shape around the utilised area and filtering the result to reduce noise, the decision to use only one half of the film thickness map can be taken. Finally, a 3D surface plot of the whole film thickness matrix (Figure 10(a)) and two 2-dimensional plots of perpendicular

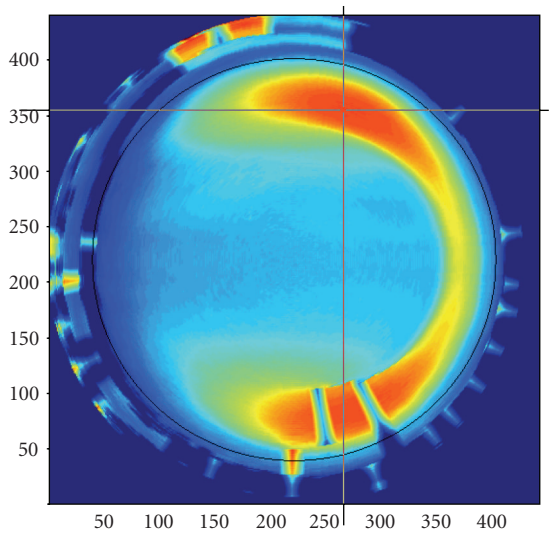

Figure 9: Selection of the useful area (black circle) and the point of minimum film thickness (cross point).

sections through the central point are created (Figures 10(b) and 10(c)) (the ripple in the central region could be related to the filtering level chosen for this example). This allows the user to check if the results are plausible by comparing also with a theoretical indication output obtained using standard film thickness formulas [18]. In this example, one half of the contact has been used. Finally, the result file and the plots will be saved.

3. FILM THICKNESS RESULTS

3.1. Experimental details

The programme developed has been tested with series of images obtained with an experimental apparatus for investigation of lubricated contacts. A schematic drawing of the test rig used is shown in Figure 11. The specimen and the disc are driven by separate DC motors controlled through a LabView programme running on a standard PC. The load is applied via a lever mechanism supported on a radial gas bearing whose axial motion is constrained by a load cell for measuring the friction force. An optical interferometry system with white light and a high-speed camera is used to measure the film thickness and shape. Further details of the rig are reported in [5].

In order to investigate steady-state and transient conditions by using the programme developed for the analysis of the interference images, test conditions have been chosen producing film thickness values between 0.04 and 0.7 μm, roughly, the field of applicability of the program.

A glass disc with a SiO_2 spacer layer of 0.06 μm and an AISI52100 bearing steel ball with a diameter of 10.319 mm has been used in this work. Their root mean squares roughness are R_q = 0.01 μm and R_q = 0.007 μm, respectively. A paraffin base mineral oil (SN500) has been used as a lubricant, whose dynamic viscosity, pressure viscosity coefficient, and density are η_0 = 0.497 Pa·s, α = 2.87 10^{-8} Pa^{-1}, and

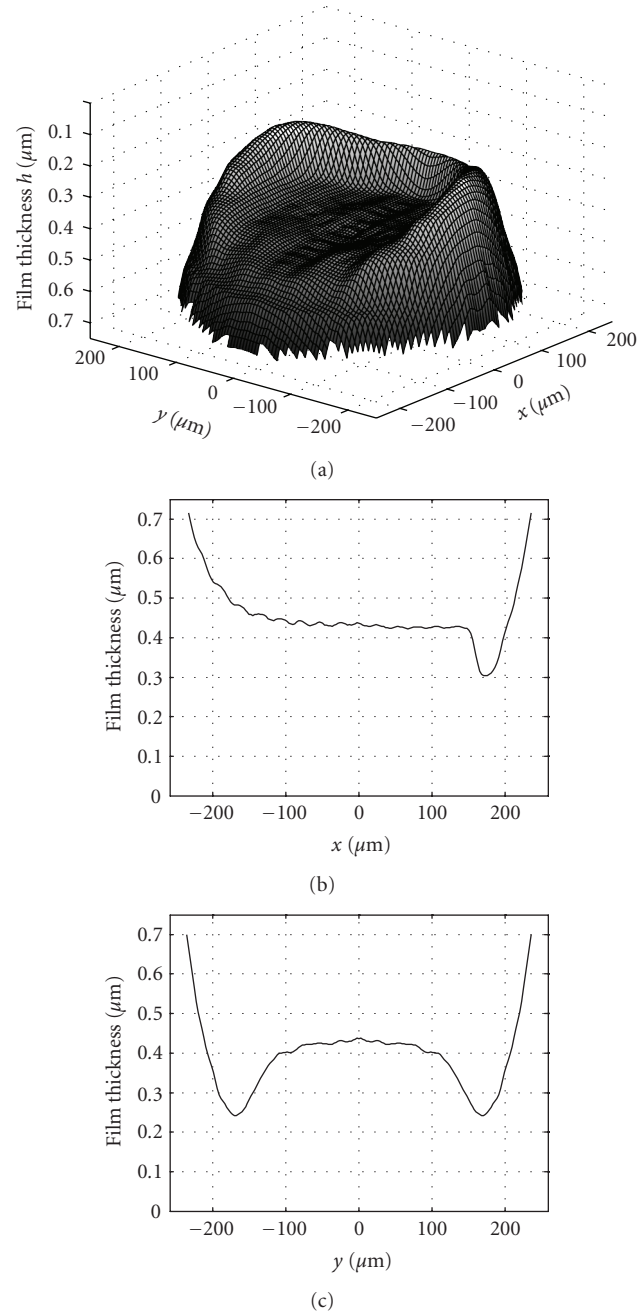

Figure 10: Final results: 3D surface plot of the film thickness (a) and film thickness in midplane sections along the x axis (entraining direction) (b) and the y axis (perpendicular to the entraining direction) (c).

ρ_0 = 892 kg/m^3 at test temperature and atmospheric pressure. The oil temperature and the load has been kept constant during all tests respectively at T = 12°C and F = 15 N (the corresponding Hertzian radius and pressure are 0.1 mm and 0.7 GPa, resp.).

Tests have been carried out under steady-state conditions for entraining velocities $u_e = (u_s + u_d)/2$ ranging from u_e = 0.025 to u_e = 0.25 ms^{-1} and different values of $S = (u_s - u_d)/u_e$ (0, ±0.8 and ±1.8) (u_s and u_d are the surface speeds of the

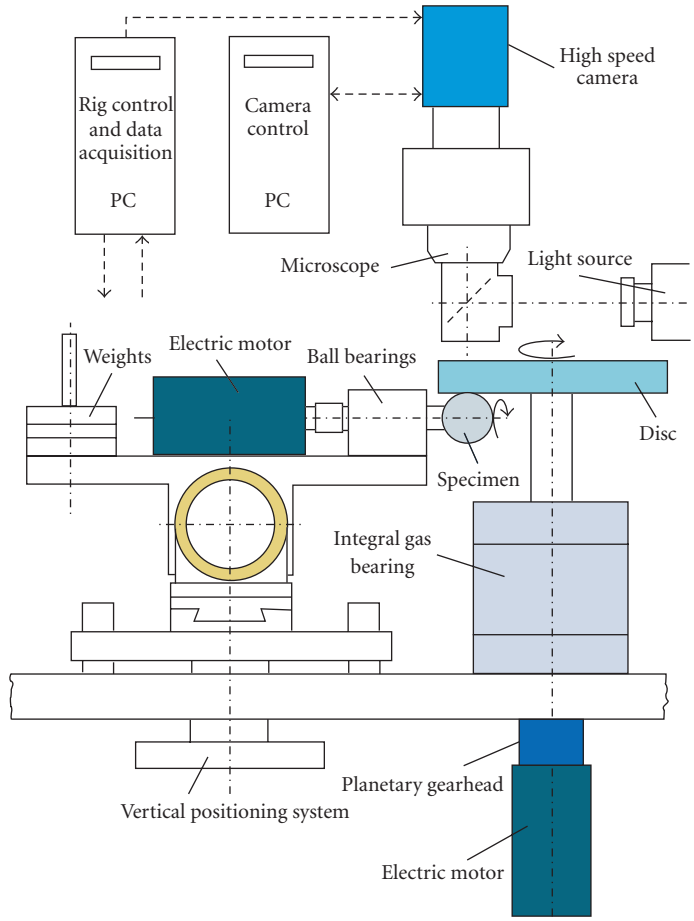

Figure 11: Schematic drawing of the test rig.

steel ball and the disc). Under transient conditions, the entraining velocity has been varied with a sinusoidal law between $u_{\min} = 0.04\,\text{ms}^{-1}$ and $u_{\max} = 0.225\,\text{ms}^{-1}$ for two frequencies of 0.25 Hz and 1 Hz.

3.2. Steady-state conditions

In Figure 12, some interferograms recorded under steady-state conditions for different values of the slide-to-roll ratio S and different velocities are shown. The oil entrainment is from the left. Such interferograms have been used as inputs of the previous described programme in order to evaluate the film thickness. However, a lot of information can be gained also by looking on the original interferograms.

As described before, in white light interferometry, the interferograms consist of multicoloured fringes with changing colours depending on the film thickness. Looking at the images of Figure 12, it can be seen that at very low entraining velocities, the interferograms are very similar in colour, independent of the slide-to-roll ratio. The horseshoe-shaped constriction at the outlet zone, which contains also the minimum film thickness, is very small and thus the colour perception is close to the central film thickness. With higher entraining velocities, the difference in colour of the horseshoe-shaped constriction and the central film thickness part is evident. Also, a clear difference can be seen between pure rolling conditions (S = 0) and rolling-sliding conditions at different S. At the highest entraining velocity and slide-to-roll ratio, also a difference in colour is evident between S = −1.8 and S = +1.8. These qualitative observations should be quantitatively evident in the film thickness results after analysing the interferograms by the automatic digital image processing programme.

Some sample results are shown in Figure 13. The highest film thickness is found under pure rolling conditions (S = 0). At high positive values of S the EHL contact appears flattened compared to high negative values, where a large difference between minimum and central film thickness emerges. It must be annotated that this asymmetry seems to occur only in contacts between materials with different thermal properties [19].

The results obtained for the other values of S and u_e confirm the reduction of the film thickness for $S \neq 0$ compared to pure rolling conditions. In addition, it appears that the film thickness diminishes more for positive than for negative S and that these effects diminish with low entraining velocities.

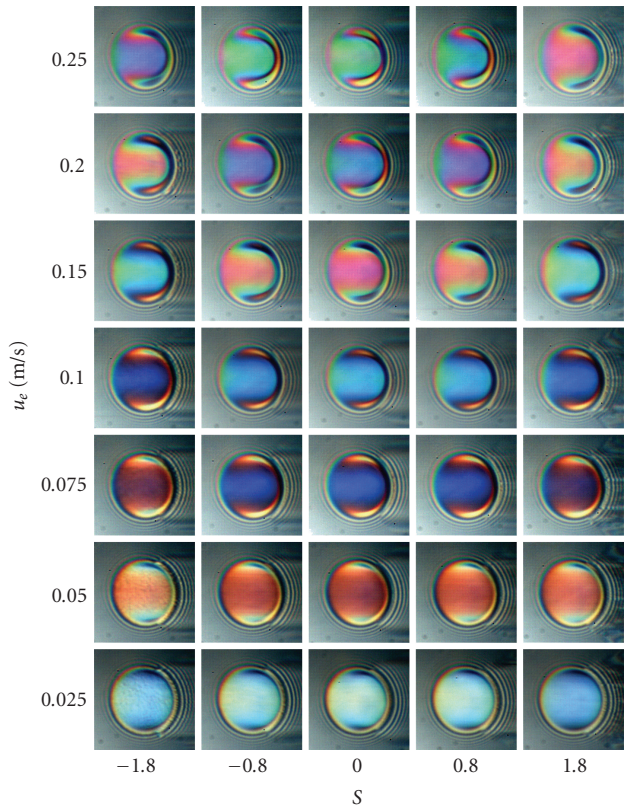

Figure 12: Interferograms obtained under steady-state conditions.

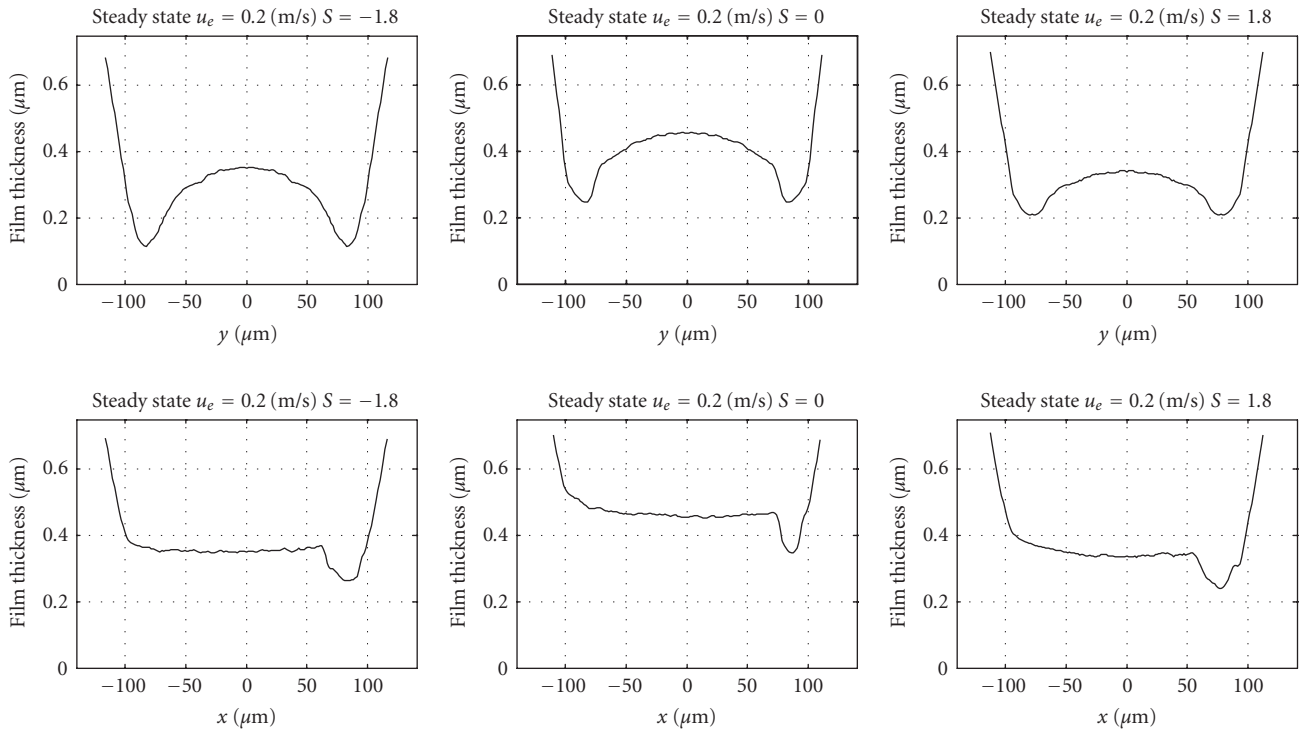

Figure 13: Film thickness profiles along the y- (top) and x-directions (bottom) (perpendicular to the entraining direction and entraining direction, resp.) under steady-state conditions for S = −1.8, S = 0, and S = +1.8.

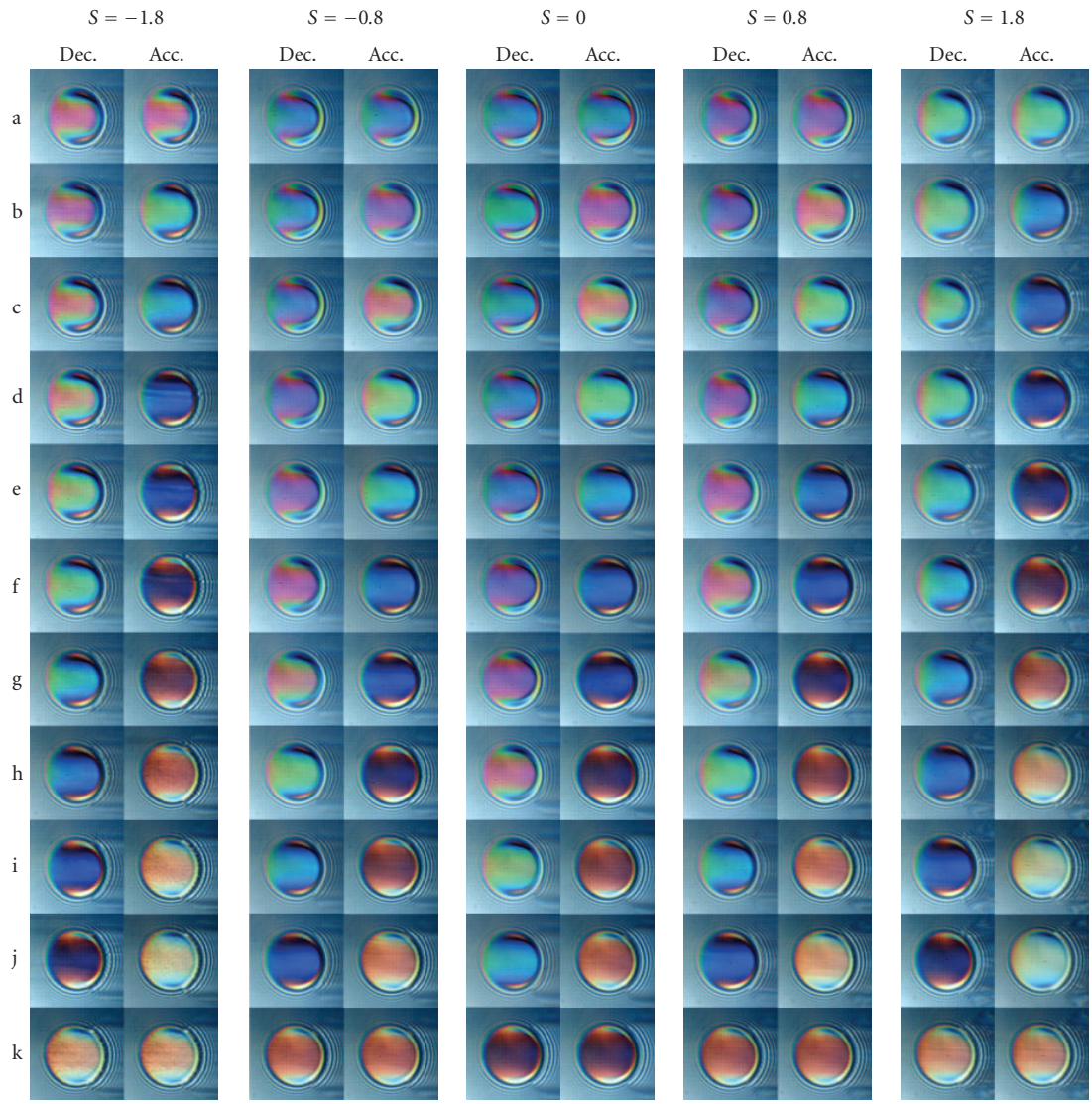

Figure 14: Interferograms obtained under transient conditions. Test frequency: 0.25 Hz. (Entraining velocities u_e: a = 0.2250, b = 0.2065, c = 0.1880, d = 0.1695, e = 0.1510, f = 0.1325, g = 0.1140, h = 0.0955, i = 0.0770, j = 0.0585, k = 0.0400 m/s).

These results are in agreement with the behaviour found in [3].

3.3. *Transient conditions*

The interferograms recorded under transient conditions at the two frequencies of 0.25 Hz and 1 Hz are shown in Figures 14 and 15, respectively. For each value of S, the interference images recorded during one cycle are reported in two columns, starting from the highest speed at the top of the column on the left to the lowest one at the bottom (decelerating conditions, Dec), and coming back from the lowest speed to the highest one at the top of the column on the right (accelerating conditions, Acc). Only for clarity reasons, the interference images recorded at the lowest speeds are repeated twice.

Some aspects are immediately evident by the simple visual analysis of these images.

The different interferograms obtained for the same velocities under decelerating and accelerating conditions clearly indicate a shift between the speed and the film thickness variations. The differences are more evident for the highest test frequency.

Differences are also evident between film thicknesses for positive and negative values of S as found for the steady-state conditions.

Quantitative results obtained using the programme developed are shown in Figures 16 and 17. Due to the big amount of plots obtained, results have been summarised in diagrams showing the trends of the measured values of the minimum and central film thickness for the different values of *S*.

Figure 16 shows the measured central film thickness, h_{cen}, plotted as a function of time and entraining speed. The interpolated values under steady-state conditions are reported for comparison too.

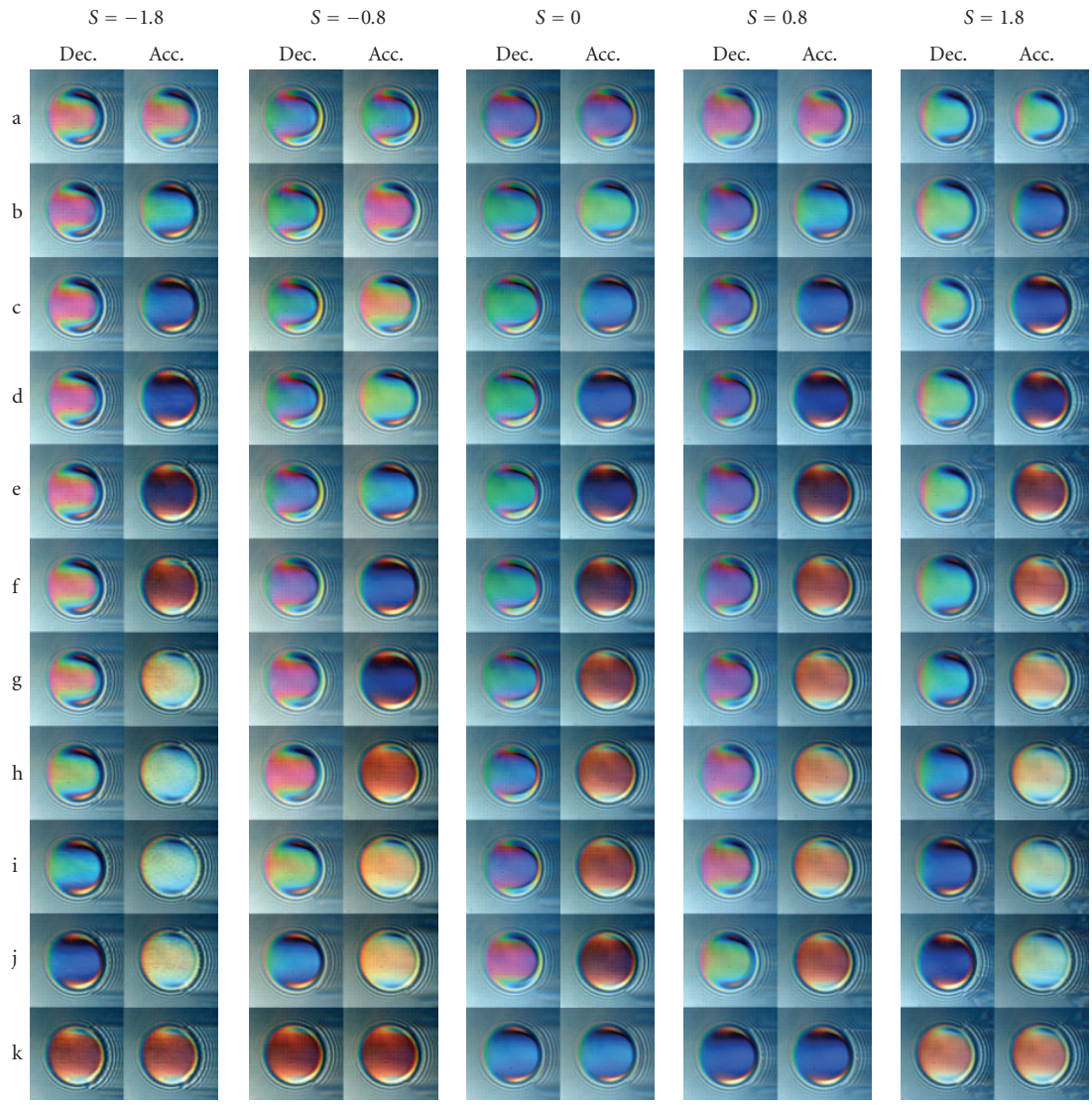

Figure 15: Interferograms obtained under transient conditions. Test frequency: 1 Hz. (Entraining velocities u_e: a = 0.2250, b = 0.2065, c = 0.1880, d = 0.1695, e = 0.1510, f = 0.1325, g = 0.1140, h = 0.0955, i = 0.0770, j = 0.0585, k = 0.0400 m/s).

The values under steady-state conditions were also compared with the theoretical ones showing a general good agreement for central film thicknesses corresponding to the part of the calibration curve above the step observed between 0.16 μm and 0.24 μm (see Figure 6). For h_{cen} greater than about 0.2 μm, the slope of the h_{cen}-velocity line in a log-log scale is about 0.7, according to the EHL theory [18].

For an immediate comparison among the results obtained with the different values of S under transient conditions, central and minimum film thickness for the two frequencies are also shown for different values of S in Figure 17. The gross lines refer to the central film thicknesses and the thin lines refer to the minimum film thicknesses, while the solid lines refer to the film thicknesses obtained at test frequency of 1 Hz and the dashed lines refer to the test frequency of 0.25 Hz. The arrows show the direction of the entraining speed (higher film thicknesses correspond to decelerating speed and lower film thicknesses to accelerating speed).

Some preliminary considerations are reported here, while more detailed explanations of the results are reported in [20].

Due to squeeze effects, the film thickness values are usually higher for decreasing velocity than under steady-state conditions, whereas for increasing velocity they are lower, respectively. Due to the higher accelerations, this effect is greater for the test frequency of 1 Hz than for 0.25 Hz. At 1 Hz, this hysteresis behaviour is so strong that the most extreme film thicknesses do not coincide with the extremes of the entraining velocity and film thicknesses continue to increase while velocity is already decreasing and reach their maximum only a few measuring points later. When the

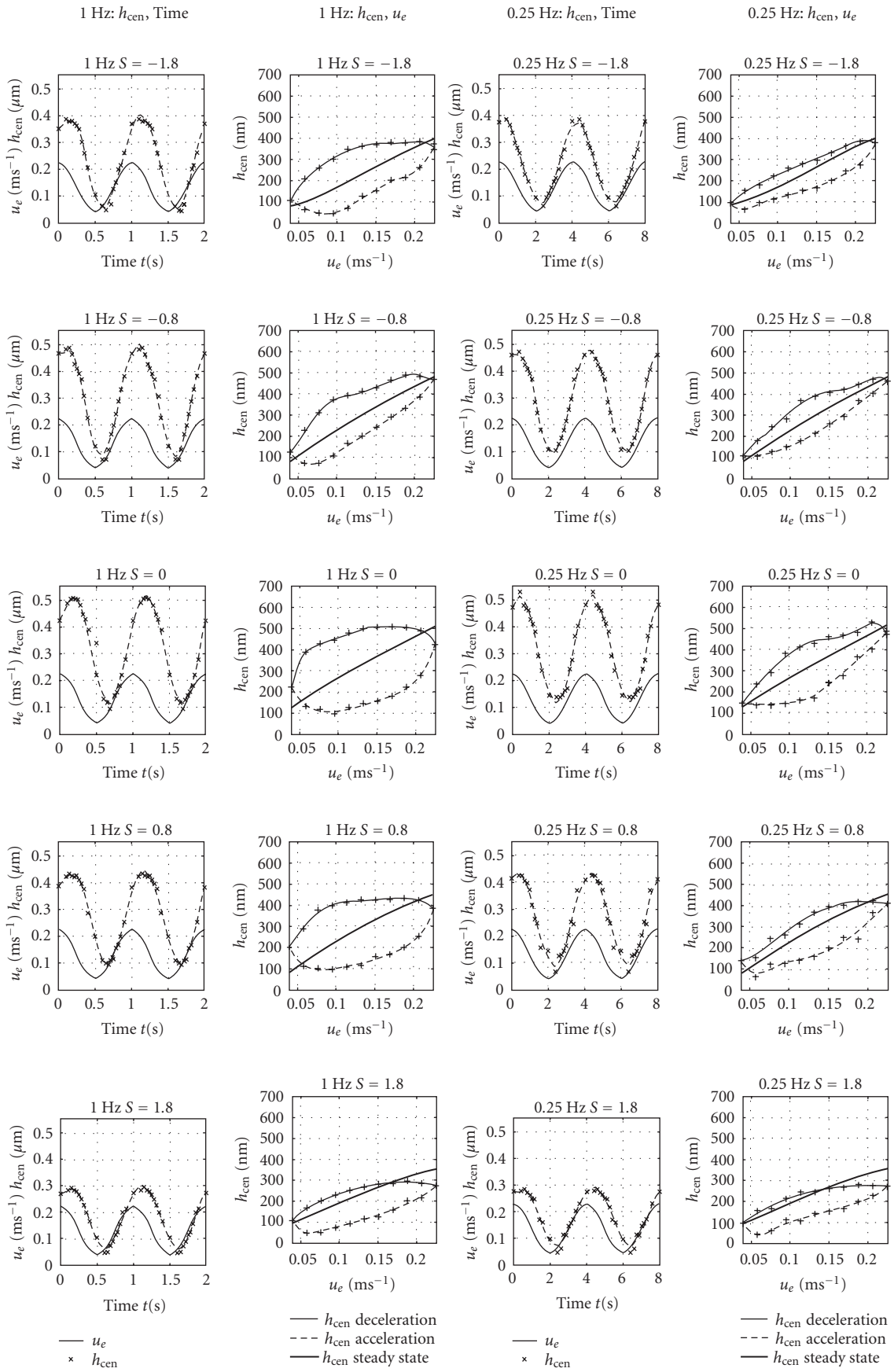

Figure 16: Central film thickness as a function of time and entraining velocity for the two test frequencies 1 Hz and 0.25 Hz.

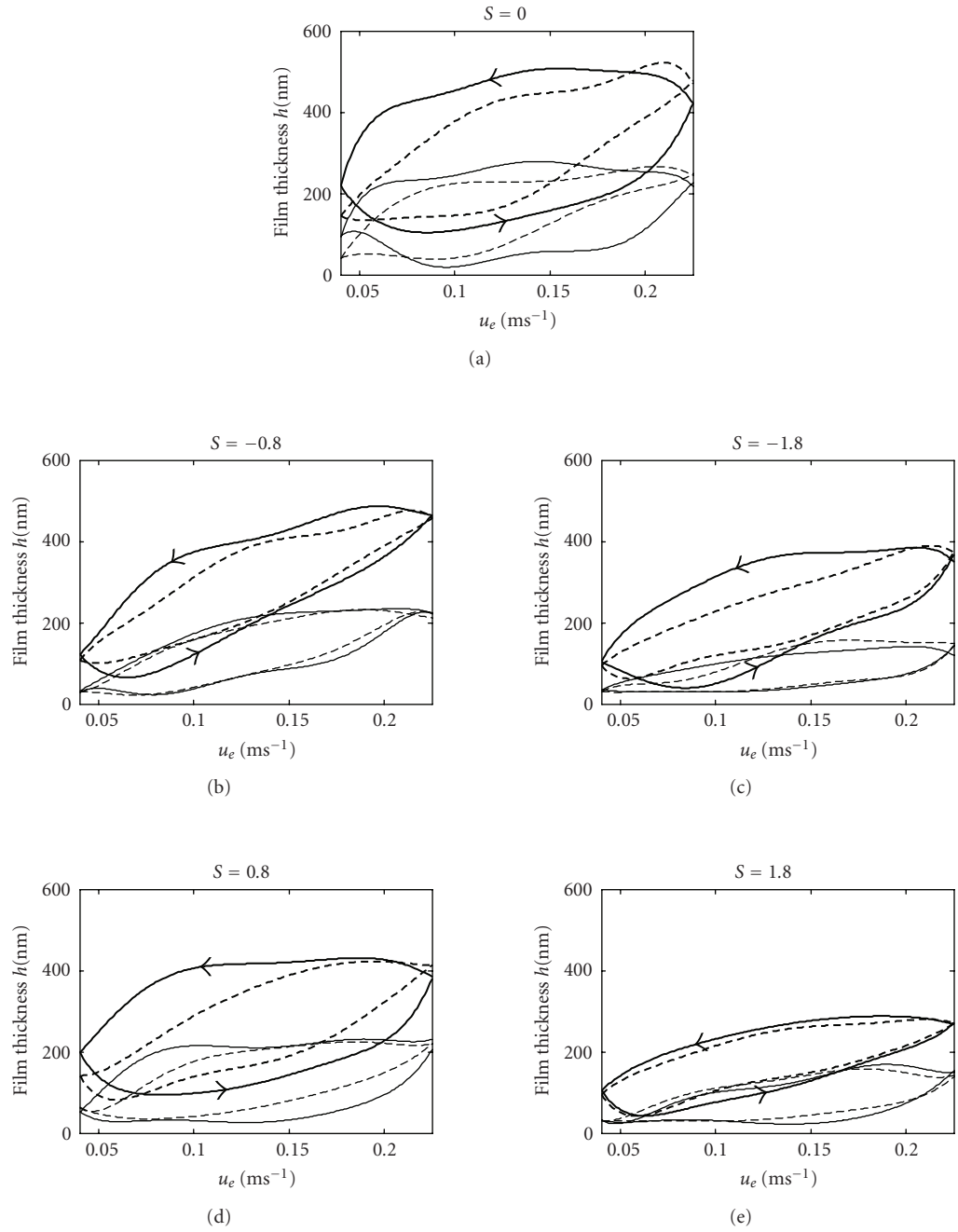

Figure 17: Central (thick lines) and minimum (thin lines) film thickness for 0.25 Hz (dashed lines) and 1 Hz (solid lines) for different values of S: S = 0 (a), S = −0.8 (b), S = −1.8 (c), S = +0.8 (d), and S = +1.8 (e).

entraining velocity passes its minimum, the same behaviour can be observed correspondingly. For pure rolling conditions (S = 0), the film thickness loops are bigger than for high slide-to-roll-ratios.

Similarly to the stationary conditions, the highest film thicknesses are reached for pure rolling conditions independently of the test frequency. In addition, also under transient conditions, an asymmetry is found in the film thickness results that indicate lower values of the film thickness for positive S.

4. CONCLUSIVE REMARKS AND FUTURE DEVELOPMENTS

An automated image processing programme has been developed in the Matlab environment in order to determine film thickness maps of EHL point contacts from white light interferograms. It is based on the analysis of the hue channel of interferogram images represented in HSV colour space. It has been particularly developed for processing image series comparatively easily and fast. More insights and information

in analysing white light interferograms are gained compared to standard film thickness measurements by eye where often only approximated values of the minimum and central film thickness can be given.

The measurement range is currently limited to maximum film thicknesses of 0.7 μm and could only be significantly extended by using for example trichromatic instead of white light. On a Hertzian contact, the measurement uncertainty of the method has been determined to be in the order of 0.01 μm. In EHL contacts, additional deviations of about the same scale will occur due to the pressure dependence on the refractive index of the lubricant. In future developments, this error could be corrected iteratively if a calculation of the pressure profile will be integrated into the image analysis program.

To obtain always flawless results, the quality of the images is important, and possibilities to enhance it should be tackled in the future. A different microscope and illumination system could improve the situation. However, there are also factors independent of the optical set-up that reduces image quality, such as cavitations in the outlet region of the contact.

Several algorithms to unwrap signals found in literature were tested. Finally, a custom solution, which combines a classical integration approach for the phase derivative with a coordinate transformation, was implemented. However, a more sophisticated phase unwrapping algorithm would be necessary to increase the chance of analysing also corrupted image regions successfully.

Similar solutions present in the literature might offer more accurate results, but they are not particularly focused on fast processing of many interferograms as the present programme.

The programme has been used for analysing several images recorded in tests carried out under steady-state as well as transient conditions for different slide-to-roll ratios S and different test frequencies.

The results evidenced a reduction of the film thickness when increasing the percentage of sliding compared to pure rolling conditions. This reduction occurs in an asymmetric way, both for steady-state and transient conditions, showing lower values of the central film thickness for positive S (ball running faster than the disc) than for negative S. This can be related to thermal effects such as the temperature viscosity wedge action. The temperature on the ball surface is lower in the case where the ball runs slower than the disc. For a glass-disc-on-ball configuration, thermal viscosity wedge effects usually occur under conditions of faster disc, for example, the occurrence of Kaneta's dimples [19].

High slide-to-roll ratios values seem to reduce the squeeze effect on the film thickness under transient conditions, particularly for higher test frequencies. The reduction of the amplitude of the film thickness loops is significantly higher for positive S than for negative S. This could be related again to thermal effects as the temperature viscosity wedge action. A detailed discussion on these aspects is reported in [20].

REFERENCES

[1] A. Cameron and R. Gohar, "Theoretical and experimental studies of the oil film in lubricated point contact," *Proceedings of the Royal Society of London A*, vol. 291, no. 1427, pp. 520–536, 1966.

[2] C. A. Foord, W. C. Hammann, and A. Cameron, "Evaluation of lubricants using optical elastohydrodynamics," *Tribology Transactions*, vol. 11, no. 1, pp. 31–43, 1968.

[3] M. Smeeth and H. A. Spikes, "The influence of slide/roll ratio on the film thickness of an EHD contact operating within the mixed lubrication regime," in *Proceedings of the of 23rd Leeds-Lyon Symposium on Tribology*, pp. 695–703, Elsevier, Leeds, UK, September 1996.

[4] J. Sugimura, W. R. Jones Jr., and H. A. Spikes, "EHD film thickness in non-steady state contacts," *Journal of Tribology*, vol. 120, no. 3, pp. 442–452, 1998.

[5] R. Bassani, E. Ciulli, K. Stadler, and M. Carli, "Lubricated nonconformal contacts under steady state and transient conditions," in *Proceedings of the 17th AIMETA General Conference*, Florence, Italy, September 2005.

[6] R. Bassani, E. Ciulli, M. Carli, and K. Stadler, "Experimental investigation of transient and thermal effects on lubricated non-conformal contacts," in *Proceedings of the 5th International Conference on Tribology (AITC-AIT '06)*, Parma, Italy, September 2006.

[7] R. Bassani and E. Ciulli, "Lubricant film thickness and shape using interferometry and image processing," in *Elastohydrodynamics-'96: Fundamentals and Applications in Lubrication and Traction: Proceedings of the 23rd Leeds-Lyon Symposium on Tribology (Leeds, UK)*, pp. 81–90, Elsevier, Amsterdam, The Netherlands, 1997.

[8] R. Bassani, E. Ciulli, and R. Squarcini, "A digital image processing method for geometry modeling of a EHL contact," in *Proceedings of the 16th AIMETA Congress of Theoretical and Applied Mechanics*, Ferrara, Italy, September 2003.

[9] J. Molimard, M. Querry, P. Vergne, et al., "Differential colorimetry: a tool for the analysis of fluid film lubrication," *Mécanique & Industries*, vol. 3, no. 6, pp. 571–581, 2002.

[10] O. Marklund, *Interferometric measurements and analysis with applications in elastohydrodynamic experiments*, Ph.D. thesis, Luleå University of Technology, Luleå, Sweden, 1999.

[11] M. Eguchi and T. Yamamoto, "Film thickness measurement using white light spacer interferometry and its calibration by HSV color space," in *Proceedings of the 5th International Conference on Tribology (AITC-AIT '06)*, Parma, Italy, September 2006.

[12] O. Marklund and L. Gustafsson, "Interferometry-based measurements of oil-film thickness," *Proceedings of the Institution of Mechanical Engineers, Part J: Journal of Engineering Tribology*, vol. 215, no. 3, pp. 243–259, 2001.

[13] R. S. Berns, *Billmeyer and Saltzman's Principles of Color Technology*, John Wiley & Sons, New York, NY, USA, 2000.

[14] D. C. Ghiglia and L. A. Romero, "Robust two-dimensional weighted and unweighted phase unwrapping that uses fast transforms and iterative methods," *Journal of the Optical Society of America A*, vol. 11, no. 1, pp. 107–117, 1994.

[15] J. Tribolet, "A new phase unwrapping algorithm," *IEEE Transactions on Acoustics, Speech, and Signal Processing*, vol. 25, no. 2, pp. 170–177, 1977.

[16] A. K. Jain, *Fundamentals of Digital Image Processing*, Prentice-Hall, Upper Saddle River, NJ, USA, 1989.

[17] O. Marklund and L. Gustafsson, "Correction for pressure dependence of the refractive index in measurements of lubricant film thickness with image analysis," *Proceedings of the Institution of Mechanical Engineers, Part J: Journal of Engineering Tribology*, vol. 213, no. 2, pp. 109–126, 1999.

[18] B. J. Hamrock, *Fundamentals of Fluid Film Lubrication*, Mcgraw-Hill, New York, NY, USA, 1994.

[19] M. Kaneta and P. Yang, "Effects of thermal conductivity of contacting surfaces on point EHL contacts," *Journal of Tribology*, vol. 125, no. 4, pp. 731–738, 2003.

[20] E. Ciulli, K. Stadler, and T. Draexl, "The influence of the slide-to-roll ratio on the friction coefficient and film thickness of EHD point contacts under steady state and transient conditions," in *Proceedings of the European Conference on Tribology and Final Conference of COST 532 Action (ECOTRIB '07)*, vol. 1, pp. 389–400, Ljubljana, Slovenia, June 2007.